The 9th European Congress on Computational Methods in Applied Sciences and Engineering
ECCOMAS Congress 2024
3–7 June 2024, Lisboa, Portugal

A HYBRID HEXAHEDRAL SOLID-SHELL ELEMENT WITH SELF-EQUILIBRATED STRESSES FOR THE GEOMETRICALLY NONLINEAR STATIC ANALYSIS OF COMPOSITE LAMINATED STRUCTURES

Giovanni Zucco[1], Francesco S. Liguori[2] and Antonio Madeo[2]

[1] University of Limerick
School of Engineering and Bernal Institute
Limerick, Ireland
e-mail: giovanni.zucco@ul.ie

[2] University of Calabria
DIMES, Ponte P. Bucci, Cubo 42 B
87036 Rende (Cosenza), Italy
e-mail: francesco.liguori@unical.it and antonio.madeo81@unical.it

Key words: Geometrically nonlinear analysis, FEM, Hybrid finite elements, Solid-shell elements

Summary. Hybrid finite elements with self-equilibrated assumed stresses have proven to provide several advantages for analysing shell structures. They guarantee high performance when using coarse meshes and accurately represent the stress field. Additionally, they do not require assumptions about the displacement field within the element domain, and the integration is efficiently performed only along their contours. This work exploits those advantages to develop a solid-shell finite element for the geometrically nonlinear static analysis of composite laminated structures. In particular, an eight-node finite element, which has 24 displacement variables and 18 stress parameters, is developed. The displacement field is described only by translations, eliminating the need for complex finite rotation treatments in large displacement problems. A Total Lagrangian formulation is used with the Green-Lagrange strain tensor and the second Piola-Kirchhoff stress tensor. Thickness locking is cured using an assumed natural strain formulation for the transversal normal stress, and the assumed stress field eliminates shear locking. Then, for the analysis of linear-elastic problems, no domain integration is needed, and all the element operators are obtained by line integrals. The resulting formulation is efficient and allows for easy implementation. Computed numerical results show the accuracy and robustness of the presented element when used for both the linear elastic static and geometrically nonlinear elastic static analysis of composite laminated shell structures.

1 INTRODUCTION

Shells are widely used in many engineering structures due to the possibility of designing them with complex shapes, allowing for efficient and optimised performance [17, 5]. Because of their high slenderness ratios, many shell structures require consideration of geometric nonlinearities to assess their response to compressive stresses accurately [9]. Therefore, studying shell structures undergoing large displacements requires efficient and robust methods. Over time, research on the

Finite Element (FE) method has led to the development of several elements based on shell models whose kinematic is described using the translation and rotation of the mid-plane. However, when modelling shells that experience large displacements, finite 3D rotation algebra is necessary, which results in complex formulations [21, 2]. In this regard, solid-shell elements are an appealing alternative to traditional shell models because their kinematics can be described only through translations [4, 10]. In fact, starting from a three-dimensional description at the continuum level, solid-shell models are developed by interpolating the displacements along the thickness of the shell, resulting in generalised strain and stress fields that depend on the midplane coordinates [19]. Solid-shell models require a three-dimensional representation of the structure's geometry allowing more accurate modelling of the geometry, boundary conditions, and connections and the combined use of solid-shell and brick elements. Despite their advantages, solid-shell elements are affected by different types of interpolation-locking phenomena such as transverse shear- [1, 6], trapezoidal- [16, 18], and thickness-locking [20, 4].

Solid-shell elements derived from the Hellinger-Reissner variational principle have shown significant advantages over their displacement-based counterparts. For example, mixed solid-shell elements using the Green-Langrange strain measures within a Total Lagrangian framework have shown to be robust and efficient formulations whose mixed energy cubically depends on the stress and displacement parameters, thereby obtaining shallow levels of nonlinearity and, therefore, simplified evaluations of the strain energy variations [14]. This aspect is particularly appealing when using reduced-order models, such as those based on Koiter's theory of stability, which use energy variations up to the fourth order [11]. To further improve the accuracy of a mixed formulation, the assumed stresses can be selected to satisfy some governing equations a priori. For example, the hybrid-Trefftz FEs in shell models are based on assumed stresses that satisfy equilibrium and compatibility equations in the linear elastic case [3]. For this kind of elements, assuming the displacement interpolation inside its domain is unnecessary, and, therefore, their compatibility-equilibrium and compliance operators are obtained through integration along the element's contour.

This work presents a mixed solid-shell hexahedral element for the geometrically nonlinear analysis of elastic shells. We named this element MISS-4S, which stands for Mixed Isostatic Self-Stress equilibrated, four nodes, Solid-shell. The element has six translational Degrees Of Freedom (DOFs) at each vertex of the solid-shall midplane. The displacement and position fields are a re-parameterisation of an eight-node hexahedron with three DOFs per node. A simple bilinear interpolation describes all the displacement components. To be isostatic, MISS-4S has 18 stress parameters, selected by imposing the equilibrium equations of the generalised stresses on a Cartesian frame for small displacements and zero bulk loads. Then, equilibrium is satisfied for all the element distorted configurations. A local elemental Cartesian system ensures the objectivity of the stress field assumptions and reduces the sensitivity to mesh distortions. The Green-Lagrange strain measure is adopted within a Total Lagrangian approach. The trapezoidal locking is cured using the ANS approach, while the modified generalised stiffness matrix [18] is adopted to remove thickness locking. The mixed formulation eliminates shear and volumetric locking, typical of the displacement-based formulation. The main difference that MISS-4S presents with respect to other solid-shell elements in the literature, is that its stress fields satisfy the equilibrium equations in the linear elastic case and for zero bulk loads. In this work, MISS-4S is implemented within a path-following strategy that uses the Riks method to solve geometrically nonlinear problems. The reliability of MISS-4S is shown through numerical tests that compare its results

for geometrically nonlinear problems with those obtained with the element in [18].

2 THEORY

This Section presents a brief recall of the theory beyond the development of MISS-4S. Further insights on the formulation of MISS-4S for isotropic structures can be found in [8].

2.1 Element geometry and reference systems

MISS-4S has a hexahedral geometry with four nodes at its top surface and four at its bottom surface. Then, four nodes coincident with the vertexes laying on the middle plane are considered whose coordinates are described by $\boldsymbol{X}_{0i}$ and $\boldsymbol{X}_{ni}$, with $i = 1, \dots 4$. The vector $\boldsymbol{X}_e$ collects the element coordinates as

$$\boldsymbol{X}_e = \begin{bmatrix} \boldsymbol{X}_{0e} \\ \boldsymbol{X}_{ne} \end{bmatrix}, \quad \boldsymbol{X}_{0e} = \begin{bmatrix} \boldsymbol{X}_{01} \\ \boldsymbol{X}_{02} \\ \boldsymbol{X}_{03} \\ \boldsymbol{X}_{04} \end{bmatrix}, \quad \boldsymbol{X}_{ne} = \begin{bmatrix} \boldsymbol{X}_{n1} \\ \boldsymbol{X}_{n2} \\ \boldsymbol{X}_{n3} \\ \boldsymbol{X}_{n4} \end{bmatrix}. \tag{1}$$

The element has three Cartesian system (see Fig. 1). A local Cartesian system $\{o_0, z_1, z_2, z_3\}$ is defined over the element mid-surface, with z_3 aligned with the element thickness direction. Then, a further local Cartesian system $\{o, x_1, x_2, x_3\}$, translated and rotated with respect to the initial local Cartesian system exists. Finally, a global Cartesian system ($\{O, X_1, X_2, X_3\}$) describes the geometry within the three-dimensional space and allows standard assemblage FE procedures.

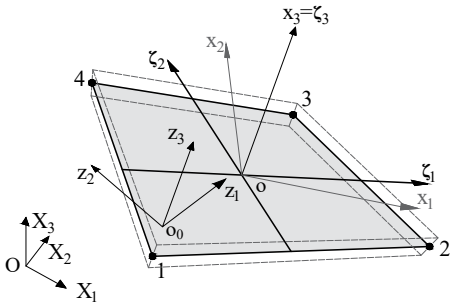

Figure 1: MISS-4S geometry and reference systems: global 3D Cartesian ($\{O, X_1, X_2, X_3\}$), initial local ($\{o_0, z_1, z_2, z_3\}$), rotated local ($\{o, x_1, x_2, x_3\}$), and internal ($\{o, \zeta_1, \zeta_2, \zeta_3\}$) coordinate systems.

The in-plane coordinates of the dimensionless internal system $\{\zeta_1, \zeta_2\}$ are implicitly defined by

$$\begin{cases} z_1 = A_0 + A_1\zeta_1 + A_2\zeta_1\zeta_2 + A_3\zeta_2 \\ z_2 = B_0 + B_1\zeta_1 + B_2\zeta_1\zeta_2 + B_3\zeta_2 \end{cases}, \quad \begin{bmatrix} A_0 & B_0 \\ A_1 & B_1 \\ A_2 & B_2 \\ A_3 & B_3 \end{bmatrix} = \frac{1}{4} \begin{bmatrix} 1 & 1 & 1 & 1 \\ -1 & 1 & 1 & -1 \\ 1 & -1 & 1 & -1 \\ -1 & -1 & 1 & 1 \end{bmatrix} \begin{bmatrix} z_{11} & z_{21} \\ z_{12} & z_{22} \\ z_{13} & z_{23} \\ z_{14} & z_{24} \end{bmatrix}, \tag{2}$$

where $\{z_{1i},\, z_{2i}\}$, $i = 1, \ldots, 4$, are the nodal coordinates in the initial local system $\{o_0, z_1,\, z_2,\, z_3\}$. To define the rotated local Cartesian system $\{o, x_1, x_2, x_3\}$, a Jacobian matrix $\boldsymbol{J}_0$ is introduced

$$\boldsymbol{J}_0 = \begin{bmatrix} z_{1,1} & z_{1,2} \\ z_{2,1} & z_{2,2} \end{bmatrix} = \begin{bmatrix} (A_1 + A_2\zeta_2) & (A_3 + A_2\zeta_1) \\ (B_1 + B_2\zeta_2) & (B_3 + B_2\zeta_1) \end{bmatrix}. \tag{3}$$

An average Jacobian $\bar{\boldsymbol{J}}_0$ is evaluated as

$$\bar{\boldsymbol{J}}_0 = \frac{1}{4}\int_{-1}^{1}\int_{-1}^{1} \boldsymbol{J}_0 \,\mathrm{d}\zeta_1 \,\mathrm{d}\zeta_2 = \begin{bmatrix} A_1 & A_3 \\ B_1 & B_3 \end{bmatrix}, \tag{4}$$

which is decomposed into an orthogonal matrix $\boldsymbol{R}$ and a symmetric one $\bar{\boldsymbol{J}}$, so that

$$\bar{\boldsymbol{J}}_0 = \boldsymbol{R}\,\bar{\boldsymbol{J}} \quad , \quad \begin{cases} \boldsymbol{R} = \begin{bmatrix} \cos\alpha & -\sin\alpha \\ \sin\alpha & \cos\alpha \end{bmatrix}, \quad \alpha = \arctan\left(\dfrac{A_3 - B_1}{A_1 + B_3}\right) \\ \bar{\boldsymbol{J}} = \begin{bmatrix} a & c \\ c & b \end{bmatrix} = \boldsymbol{R}^T\bar{\boldsymbol{J}}_0 \end{cases}. \tag{5}$$

The rotated local Cartesian system $\{o, x_1, x_2, x_3\}$ has its origin in the element centroid o ($\zeta_1 = \zeta_2 = 0$) and is rigidly rotated through $\boldsymbol{R}$ with respect to $\{o_0, z_1, z_2, z_3\}$. Finally, the $\{x_1, x_2\}$ coordinates are defined by the following expression

$$\begin{bmatrix} x_1 \\ x_2 \end{bmatrix} = \boldsymbol{R}^T \begin{bmatrix} z_1 - A_0 \\ z_2 - B_0 \end{bmatrix}. \tag{6}$$

2.2 Assumed kinematics

The kinematics are interpolated through the same bilinear functions describing the element geometry. In particular, bilinear interpolation functions describe the element geometry as

$$\boldsymbol{X}[\boldsymbol{\zeta}] = \boldsymbol{N}_d[\boldsymbol{\zeta}]\boldsymbol{X}_e, \tag{7}$$

where $\boldsymbol{N}_d[\boldsymbol{\zeta}]$ collects the interpolation functions $\boldsymbol{N}[\boldsymbol{\zeta}_0]$ as

$$\boldsymbol{N}_d[\boldsymbol{\zeta}] \equiv \left[\boldsymbol{N}[\boldsymbol{\zeta}_0], \zeta_3\boldsymbol{N}[\boldsymbol{\zeta}_0]\right]. \tag{8}$$

$\boldsymbol{N}[\boldsymbol{\zeta}_0]$ depend on the middle surface coordinates only

$$\boldsymbol{N} = \begin{bmatrix} N_1 & \cdot & \cdot & N_2 & \cdot & \cdot & N_3 & \cdot & \cdot & N_4 & \cdot & \cdot \\ \cdot & N_1 & \cdot & \cdot & N_2 & \cdot & \cdot & N_3 & \cdot & \cdot & N_4 & \cdot \\ \cdot & \cdot & N_1 & \cdot & \cdot & N_2 & \cdot & \cdot & N_3 & \cdot & \cdot & N_4 \end{bmatrix}, \tag{9}$$

in which

$$\begin{aligned} N_1 &= \frac{1}{4}(1-\zeta_1)(1-\zeta_2), \quad N_2 = \frac{1}{4}(1+\zeta_1)(1-\zeta_2), \\ N_3 &= \frac{1}{4}(1+\zeta_1)(1+\zeta_2), \quad N_4 = \frac{1}{4}(1-\zeta_1)(1+\zeta_2). \end{aligned} \tag{10}$$

Therefore, the displacement fields are interpolated as

$$\boldsymbol{d}[\boldsymbol{\zeta}] = \boldsymbol{N}_d[\boldsymbol{\zeta}]\boldsymbol{d}_e, \tag{11}$$

where $\boldsymbol{d}_e$ collects the displacements of the nodes on the middle plane

$$\boldsymbol{d}_e = \begin{bmatrix} \boldsymbol{d}_{0e} \\ \boldsymbol{d}_{ne} \end{bmatrix}, \quad \boldsymbol{d}_{0e} = \begin{bmatrix} \boldsymbol{d}_{01} \\ \boldsymbol{d}_{02} \\ \boldsymbol{d}_{03} \\ \boldsymbol{d}_{04} \end{bmatrix}, \quad \boldsymbol{d}_{ne} = \begin{bmatrix} \boldsymbol{d}_{n1} \\ \boldsymbol{d}_{n2} \\ \boldsymbol{d}_{n3} \\ \boldsymbol{d}_{n4} \end{bmatrix}. \tag{12}$$

Finally, the Green-Lagrange covariant strain components are

$$\bar{\boldsymbol{\varepsilon}} = \left(\boldsymbol{\mathcal{L}}[\boldsymbol{\zeta}] + \frac{1}{2} \boldsymbol{\mathcal{Q}}[\boldsymbol{\zeta}, \boldsymbol{d}_e] \right) \boldsymbol{d}_e, \tag{13}$$

where both $\boldsymbol{\mathcal{L}}[\boldsymbol{\zeta}] \equiv \boldsymbol{\mathcal{Q}}[\boldsymbol{\zeta}, \boldsymbol{X}_e]$ and $\boldsymbol{\mathcal{Q}}[\boldsymbol{\zeta}, \boldsymbol{d}_e]$ linearly depend on $\boldsymbol{d}_e$ [7] as

$$\boldsymbol{\mathcal{Q}}[\boldsymbol{\zeta}, \boldsymbol{d}_e] \equiv \begin{bmatrix} \boldsymbol{d}_e^T \boldsymbol{N}_{d,1}^T \boldsymbol{N}_{d,1} \\ \boldsymbol{d}_e^T \boldsymbol{N}_{d,2}^T \boldsymbol{N}_{d,2} \\ \boldsymbol{d}_e^T (\boldsymbol{N}_{d,1}^T \boldsymbol{N}_{d,2} + \boldsymbol{N}_{d,2}^T \boldsymbol{N}_{d,1}) \\ \boldsymbol{d}_e^T \boldsymbol{N}_{d,3}^T \boldsymbol{N}_{d,3} \\ \boldsymbol{d}_e^T (\boldsymbol{N}_{d,3}^T \boldsymbol{N}_{d,2} + \boldsymbol{N}_{d,2}^T \boldsymbol{N}_{d,3}) \\ \boldsymbol{d}_e^T (\boldsymbol{N}_{d,1}^T \boldsymbol{N}_{d,3} + \boldsymbol{N}_{d,3}^T \boldsymbol{N}_{d,1}) \end{bmatrix}. \tag{14}$$

2.3 Assumed natural strains

Solid-shell formulations with assumed kinematics suffer trapezoidal locking phenomena [18], typically occurring when the element has a trapezoidal geometry. To avoid this phenomen, MISS-4S uses an ANS formulation, that is based on a redefinition of the transverse normal strain ε_{33} which is interpolated on the values obtained in the mid-plane nodes. Furthermore, the ANS formulation is applied to shear forces as in [18], that are interpolated on the values at the middle of each element edge, leading to the following strain redefinition

$$\begin{cases} \bar{\varepsilon}_{33} = \bar{\varepsilon}_{33}[-1,-1,0]N_1 + \bar{\varepsilon}_{33}[-1,1,0]N_2 + \bar{\varepsilon}_{33}[1,1,0]N_3 + \bar{\varepsilon}_{33}[1,-1,0]N_4 \\ \bar{\varepsilon}_{13} = \dfrac{1-\zeta_2}{2}\bar{\varepsilon}_{13}[0,-1,0] + \dfrac{1+\zeta_2}{2}\bar{\varepsilon}_{13}[0,1,0] \\ \bar{\varepsilon}_{23} = \dfrac{1-\zeta_1}{2}\bar{\varepsilon}_{23}[-1,0,0] + \dfrac{1+\zeta_1}{2}\bar{\varepsilon}_{23}[1,0,0] \end{cases}, \tag{15}$$

where $N_1 ... N_4$ are defined in Eq. (10).

2.4 Assumed stress interpolations

For a flat solid-shell reference configuration, the equilibrium equations in the linear case and for zero bulk loads can be expressed as

$$\begin{cases} \mathcal{D}_m^T \boldsymbol{\mathcal{N}} = \boldsymbol{0} \\ \mathcal{D}_b^T \boldsymbol{\mathcal{M}} - \boldsymbol{\mathcal{T}} = \boldsymbol{0} \\ \mathcal{D}_t^T \boldsymbol{\mathcal{T}} = \boldsymbol{0} \\ \mathcal{D}_3 \sigma_{33} = 0 \end{cases} \tag{16}$$

where the differential operators are

$$\mathcal{D}_m = \begin{bmatrix} \partial/\partial x_1 & \cdot \\ \cdot & \partial/\partial x_2 \\ \partial/\partial x_2 & \partial/\partial x_1 \end{bmatrix}, \quad \mathcal{D}_s = \begin{bmatrix} \partial/\partial x_1 \\ \partial/\partial x_2 \end{bmatrix}, \quad \mathcal{D}_b = \mathcal{D}_m, \quad \mathcal{D}_3 = \partial/\partial x_3. \tag{17}$$

It can be observed how, as in the shell case [12], the equilibrium equations only couple the bending $\boldsymbol{\mathcal{M}}$ and shear $\boldsymbol{\mathcal{T}}$ generalised stresses, while the membrane components $\boldsymbol{\mathcal{N}}$ and σ_{zz} are decoupled. For this reason, it is possible to interpolate the flexural, membrane and the transverse normal stresses independently as

$$\boldsymbol{t}[x_1, x_2] = \boldsymbol{N}_t[x_1, x_2]\boldsymbol{t}_e, \tag{18}$$

where $\boldsymbol{t}_e$ are the stress parameters while the interpolation functions $\boldsymbol{N}_t[x_1, x_2]$ are grouped for the membrane, transverse normal and flexural generalised stresses

$$\boldsymbol{N}_t[x_1, x_2] = \begin{bmatrix} \boldsymbol{N}_m & \cdot & \cdot \\ \cdot & \boldsymbol{N}_3 & \cdot \\ \cdot & \cdot & \boldsymbol{N}_f \end{bmatrix}. \tag{19}$$

It is worth noting that the stress fields are assumed in the Cartesian reference system $\{x_1, x_2, x_3\}$, unlike in other mixed solid-shell FEs [18, 13]. This allows to easily satisfy Eq. (16) regardless the element geometry, as previously proposed for shell FEs [12].

In mixed assumed stress FEs, the number of stress parameters $\boldsymbol{t}_e$ has to be defined in order to guarantee element stability, that is the absence of spurious modes. A necessary condition for element stability is that the number of stress parameters should at least match the number of kinematic deformation modes n_{iso}, that is the number of displacement DOFs minus the number or rigid body motions [15]. When the number of stress parameters equals n_{iso} the mixed FE is defined *isostatic*. This condition allows to cure locking phenomena typical of solid-shell FEs, namely the shear and in-plane flexural locking [18]. The explicit expression for the interpolation functions in Eq. (19) are given in the following Sections.

2.4.1 Assumed membrane stresses

The number of in-plane DOFs is 8, while the number deformation modes is 3. Therefore, to obtain the *isostatic* condition for the membrane stresses, $n_{iso} = 8 - 3 = 5$ parameters must be defined. Following a polynomial hierarchical criterion, the stress interpolation is assumed as

$$\boldsymbol{N}_m = \begin{bmatrix} 1 & 0 & 0 & x_2 & 0 \\ 0 & 1 & 0 & 0 & x_1 \\ 0 & 0 & 1 & 0 & 0 \end{bmatrix}, \tag{20}$$

which coincides with that assumed in [18] for regular geometries and gives a constant interpolation for $\boldsymbol{\mathcal{N}}_{12}$. In this way, the in-plane flexural locking is cured by avoiding parasitic shear stresses in in-plane bending conditions.

2.4.2 Assumed flexural stresses

In the flexural case, the number of displacement DOFs is 12, while the number of rigid body motions is 3, and, therefore n_{iso} for the flexural components is 9 leading to the following interpolation

$$\boldsymbol{N}_f = \begin{bmatrix} 1 & 0 & 0 & x_1 & 0 & x_2 & 0 & x_1x_2 & 0 \\ 0 & 1 & 0 & 0 & x_1 & 0 & x_2 & 0 & x_1x_2 \\ 0 & 0 & 1 & 0 & cx_2 & x_1/c & 0 & 0 & 0 \\ 0 & 0 & 0 & 1 & c & 0 & 0 & x_2 & 0 \\ 0 & 0 & 0 & 0 & 0 & 1/c & 1 & 0 & x_1 \end{bmatrix}, \tag{21}$$

where some vectors are combined through the coefficient $c = a^2/b^2$ in order to further improve the accuracy for distorted meshes. This interpolation coincides with that obtained for the MISS-4 shell FE using a Pian filtering technique [12].

2.4.3 Assumed transverse normal stress

The transverse normal stress σ_{33} in controlled by 4 kinematic variables that generate only deformative modes. Then, 4 stress parameters are employed, leading to a bilinear stress interpolation

$$\boldsymbol{N}_3 = \begin{bmatrix} 1 & x_1 & x_2 & x_1x_2 \end{bmatrix}. \tag{22}$$

2.5 Discrete nonlinear equations

Let us consider a slender hyperelastic structure subjected to conservative loads $\boldsymbol{p}[\lambda]$ proportionally increasing with the amplifier factor λ. The nonlinear solution of that structure is expressed through the virtual work equation

$$\Phi'[\boldsymbol{u}]\,\delta\boldsymbol{u} - \lambda\hat{\boldsymbol{p}}\,\delta\boldsymbol{u} = \boldsymbol{0}, \tag{23}$$

where $\boldsymbol{u}$ is the vector collecting the configuration variables $\boldsymbol{d}$ and $\boldsymbol{t}$, $(')$ is used to express the Frechèt derivative with respect to $\boldsymbol{u}$ and $\delta\boldsymbol{u}$ is a variation of $\boldsymbol{u}$.

Equation (23) is rewritten as

$$\boldsymbol{r}[\boldsymbol{u},\,\lambda] = \boldsymbol{s}[\boldsymbol{u}] - \lambda\,\hat{\boldsymbol{p}} = \boldsymbol{0}, \tag{24}$$

where $\boldsymbol{r} : \mathbb{R}^{N+1} \to \mathbb{R}^N$ is a nonlinear vectorial function of the vector $\{\boldsymbol{u}, \lambda\} \in \mathbb{R}^{N+1}$. The internal force vector $\boldsymbol{s}[\boldsymbol{u}]$ and the reference load vector $\hat{\boldsymbol{p}}$ are defined by the energy equivalences

$$\boldsymbol{s}^T\delta\boldsymbol{u} = \Phi'[\boldsymbol{u}]\delta\boldsymbol{u}\ ,\ \ \forall\,\delta\boldsymbol{u}. \tag{25}$$

Equation (24) represents a system of N-equations and $N+1$ unknowns and defines the equilibrium path as a curve in $\mathbb{R}^{N+1}$ in the $\{\boldsymbol{u},\,\lambda\}$ space from a known initial configuration $\boldsymbol{u}_0$, corresponding to $\lambda = 0$. The tangent stiffness matrix is defined as

$$\delta\boldsymbol{u}_2^T\boldsymbol{K}[\boldsymbol{u}]\delta\boldsymbol{u}_1 = \Phi''[\boldsymbol{u}]\delta\boldsymbol{u}_1\delta\boldsymbol{u}_2\ ,\ \ \forall\,\delta\boldsymbol{u}_1, \delta\boldsymbol{u}_2, \tag{26}$$

where $\delta\boldsymbol{u}_i$ are generic variations of the configuration field $\boldsymbol{u}$.

2.6 The strain energy and its variations

The mixed energy can be expressed as a sum of element contributions as

$$\Phi[u] = \sum_e \Phi_e[u], \tag{27}$$

which is expressed as

$$\Phi_e[u] = \int_{\Omega_e} \left(\boldsymbol{t}^T \boldsymbol{e} - \frac{1}{2} \boldsymbol{t}^T \boldsymbol{C}_\rho^{-1} \boldsymbol{t} \right) d\Omega_e = \boldsymbol{t}_e^T (\boldsymbol{L}_e + \frac{1}{2} \boldsymbol{Q}_e[\boldsymbol{d}_e]) \boldsymbol{d}_e - \frac{1}{2} \boldsymbol{t}_e^T \boldsymbol{H}_e \boldsymbol{\beta}_e, \tag{28}$$

where

$$\begin{aligned} \boldsymbol{H}_e &= \int_{\Omega_e} \boldsymbol{N}_\sigma^T \boldsymbol{C}_\rho^{-1} \boldsymbol{N}_\sigma d\Omega_e, \\ \boldsymbol{L}_e &= \int_{\Omega_e} \boldsymbol{N}_\sigma^T \boldsymbol{T}_e \boldsymbol{\mathcal{L}} d\Omega_e, \\ \boldsymbol{Q}_e &= \int_{\Omega_e} \boldsymbol{N}_\sigma^T \boldsymbol{T}_e \boldsymbol{\mathcal{Q}}[\boldsymbol{d}_e] d\Omega_e, \end{aligned} \tag{29}$$

whose integrals are evaluated through a Gauss integration using 2×2 points. The dependence of the quantities on ζ_1 and ζ_2 is omitted to simplify the notation. Eq.(28) allows the expression of the strain energy as an algebraic nonlinear function of the element vector

$$\boldsymbol{u}_e = \begin{bmatrix} \boldsymbol{t}_e \\ \boldsymbol{d}_e \end{bmatrix} \tag{30}$$

related to the vector $\boldsymbol{u}$, collecting all the FE parameters, through the relation

$$\boldsymbol{u}_e = \boldsymbol{\mathcal{A}}_e \boldsymbol{u}, \tag{31}$$

where $\boldsymbol{\mathcal{A}}_e$ is an assemblage operator. Once the first and second strain energy variations are obtained as detailed in [8], the solution of the geometrically nonlinear problem is obtained using the Riks' arc-length analysis.

3 NUMERICAL RESULTS

3.1 Isotropic pinched cylinder

The first test regards the geometrically nonlinear analysis of an isotropic cylindrical shell subject to two concentrated pinching forces. Figure 2 shows the cylinder's geometry, loading and boundary conditions. The elastic modulus is $E = 3 \cdot 10^4$, while Poisson's ratio is $\nu = 0.3$. Due to the symmetry of the problem, only an octave of the structure is analysed. In the post-buckling regime, the cylinder's deformation pattern presents the formation of narrow edges whose position moves when the load multiplier increases, making this test particularly severe for shell and solid-shell models. Figure 3(a) shows the equilibrium paths obtained with a mesh having 50×50 elements from which it is observed that both MISS-4S and SZE-2002 provide similar solutions that are in good agreement with that obtained with the reference solution using the IGA approach in [7]. The solution does not change significantly at mesh refinement, as shown in Fig. 3(b). Finally, for $\lambda = 1.25$, Fig. 4 shows the heatmap of M_{11} together with the cylinder's deformed configuration.

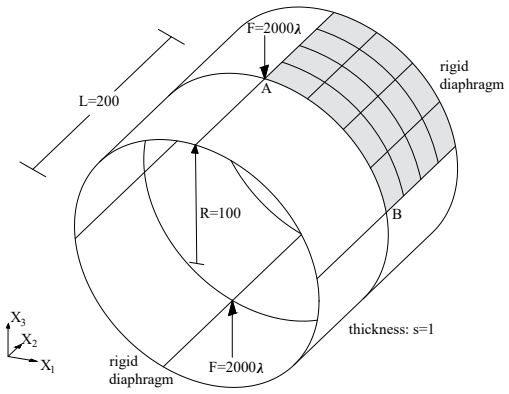

Figure 2: Pinched cylinder: geometry, loading and boundary conditions, and mesh 4×4.

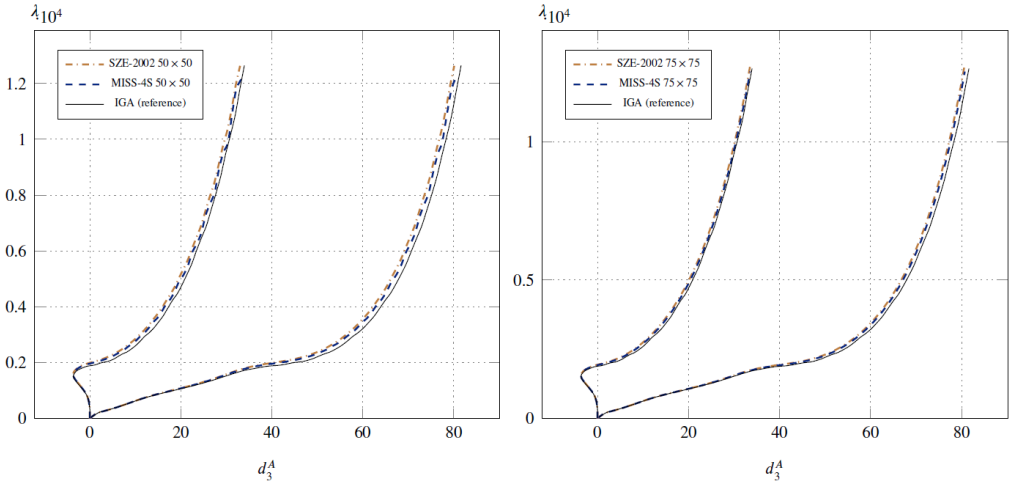

Figure 3: Pinched cylinder: equilibrium paths.

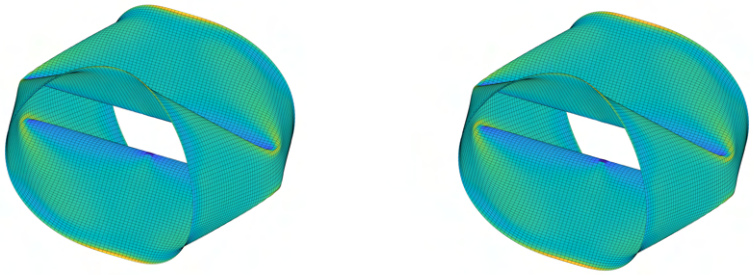

(a) MISS-4S 40×40 (b) SZE-2002 40×40

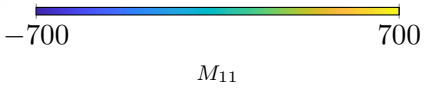

Figure 4: Pinched cylinder: heatmap of M_{11} for $\lambda = 1200$.

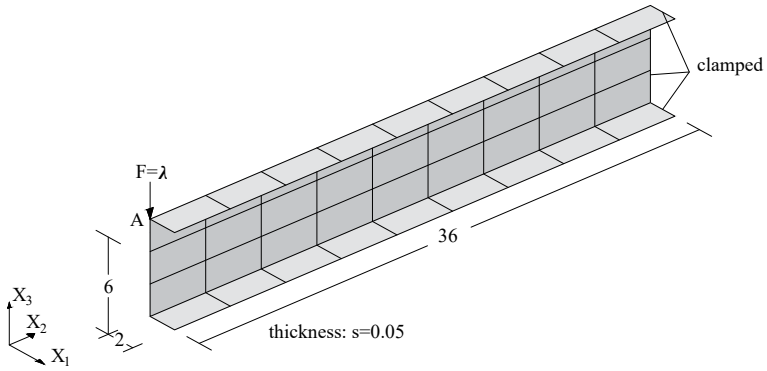

Figure 5: C-section cantilever beam: geometry, loading and boundary conditions, and mesh 5×9.

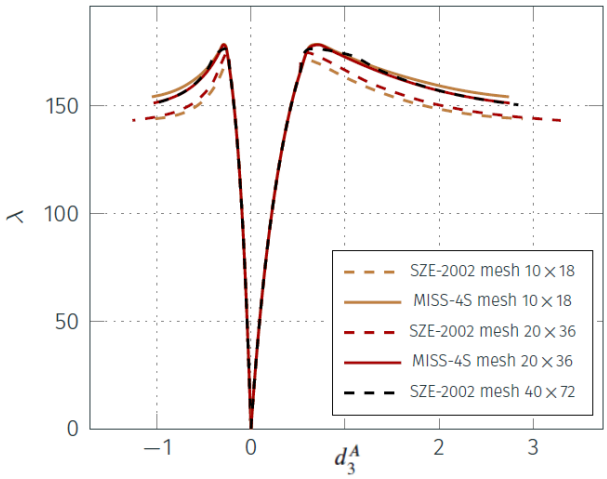

Figure 6: C-section cantilever: equilibrium path for different meshes.

3.2 Composite laminated C-section cantilever

The test analysed herein concerns a C-section cantilever beam with nodal force at its tip. Figure 5 shows the beam's geometry and loading and boundary conditions. The beam has a quasi-isotropic layup whose stacking sequence is $[0|90|\pm45]_s$. Each layer's material properties are $E_{11} = 181{\cdot}10^3$, $E_{22} = 10.27{\cdot}10^3$, $G_{12} = 7.17{\cdot}10^3$, $G_{13} = G_{23} = 5.14{\cdot}10^3$, and $\nu_{12} = 0.28$. For three different meshes, i.e. 10×18, 20×36 and 80×144, Fig. 6 shows the equilibrium curves evaluated at point A of the C-beam with the MISS-4S element and the SZE-2002 element. Equilibrium curves in Fig. 6 show that a nonlinear fundamental path and an unstable post-buckling response characterise the geometrically nonlinear behaviour of the structure under consideration. The MISS-4S element gives an accurate solution also with the coarsest mesh (10×18 elements). In contrast, the solutions obtained with the other elements present high errors in evaluating the limit load and post-buckling response. It is worth noting that a modal interaction phenomenon drives the nonlinear response of the C-beam, namely, a global torsional buckling interacts with the upper flange's local buckling, as shown in [21]. Therefore, an accurate representation of the

local buckling is required to describe its geometrically nonlinear response.

4 CONCLUSIONS

A mixed solid-shell Finite Element (FE) named MISS-4S (Mixed Isostatic Self-equilibrated Stresses 4 nodes Solid-shell) has been presented for the geometrically nonlinear analysis of composite laminated thin-walled structures. The element is derived from the Hellinger-Reissner variational principle and has 24 degrees of freedom to describe the displacement fields, while 18 stress parameters describe the stress fields. Numerical results obtained for geometrically nonlinear problems showed that the element is robust and reproduces the equilibrium paths accurately, even in the presence of high displacements and coarse meshes. Finally, this work further proves that mixed FEs with an isostatic and self-equilibrated stress representation, previously adopted in membrane and shell problems, also give advantages for solid-shell models.

REFERENCES

[1] P. M. A. Areias, J. M. A. César de Sá, C. A. Conceição António, and A. A. Fernandes. Analysis of 3d problems using a new enhanced strain hexahedral element. *International Journal for Numerical Methods in Engineering*, 58(11):1637–1682, 2003.

[2] E.J. Barbero, A. Madeo, G. Zagari, R. Zinno, and G. Zucco. Koiter asymptotic analysis of folded laminated composite plates. *Composites Part B: Engineering*, 61:267 – 274, 2014.

[3] S. Cen, Y. Shang, C.-F. Li, and H.-G. Li. Hybrid displacement function element method: a simple hybrid-trefftz stress element method for analysis of mindlin–reissner plate. *International Journal for Numerical Methods in Engineering*, 98(3):203–234, 2014.

[4] L. Leonetti D. Magisano and G. Garcea. Koiter asymptotic analysis of multilayered composite structures using mixed solid-shell finite elements. *Composite Structures*, 154:296 – 308, 2016.

[5] S. Daghighi, G. Zucco, and P. M. Weaver. Design methods for variable-stiffness super-ellipsoidal pressure vessels under thermomechanical loading. *AIAA Journal*, 61(1):475–488, 2023.

[6] F. G. Flores. Development of a non-linear triangular prism solid-shell element using ans and eas techniques. *Computer Methods in Applied Mechanics and Engineering*, 266:81–97, 2013.

[7] L. Leonetti, F. Liguori, D. Magisano, and G. Garcea. An efficient isogeometric solid-shell formulation for geometrically nonlinear analysis of elastic shells. *Computer Methods in Applied Mechanics and Engineering*, 331:159–183, 2018.

[8] F. S. Liguori, G. Zucco, and A. Madeo. A mixed hexahedral solid-shell finite element with self-equilibrated isostatic assumed stresses for geometrically nonlinear problems. *Accepted in International Journal for Numerical Methods in Engineering*, 2024.

[9] F. S. Liguori, G. Zucco, A. Madeo, G. Garcea, L. Leonetti, and P. M. Weaver. An isogeometric framework for the optimal design of variable stiffness shells undergoing large deformations. *International Journal of Solids and Structures*, 2020.

[10] F S. Liguori, G. Zucco, A. Madeo, D. Magisano, L. Leonetti, G. Garcea, and P. M. Weaver. Postbuckling optimisation of a variable angle tow composite wingbox using a multi-modal koiter approach. *Thin-Walled Structures*, 138:183–198, 2019.

[11] A. Madeo, R.M.J. Groh, G. Zucco, P.M. Weaver, G. Zagari, and R. Zinno. Post-buckling analysis of variable-angle tow composite plates using Koiter's approach and the finite element method. *Thin-Walled Structures*, 110:1–13, 2017.

[12] A. Madeo, G. Zagari, R. Casciaro, and S. De Miranda. A mixed 4-node 3d plate element based on self-equilibrated isostatic stresses. *International Journal of Structural Stability and Dynamics*, 15(4), 2015.

[13] D. Magisano, L. Leonetti, and G. Garcea. Koiter asymptotic analysis of multilayered composite structures using mixed solid-shell finite elements. *Composite Structures*, 154:296–308, 2016.

[14] D. Magisano, L. Leonetti, and G. Garcea. Advantages of the mixed format in geometrically nonlinear analysis of beams and shells using solid finite elements. *International Journal for Numerical Methods in Engineering*, 109(9):1237–1262, 2017.

[15] T. H. H. Pian and C.-C. Wu. *Hybrid and Incompatible Finite Element Methods*. Chapman & All, CRC, New-York, 1969.

[16] M. Schwarze and S. Reese. A reduced integration solid-shell finite element based on EAS and the ANS concept: Large deformation problems. *International Journal for Numerical Methods in Engineering*, (85):289–329, 2011.

[17] K. Steltner, Kriegesmann B., and C.B.W. Pedersen. Robust sizing optimization of stiffened panels subject to geometric imperfections using fully nonlinear postbuckling analyses. *Thin-Walled Structures*, 175:109195, 2022.

[18] K.Y. Sze, W.K. Chan, and T.H.H. Pian. An eight-node hybrid-stress solid-shell element for geometric non-linear analysis of elastic shells. *International Journal for Numerical Methods in Engineering*, 55(7):853–878, 2002.

[19] K.Y. Sze and L.Q. Yao. A hybrid stress ANS solid-shell element and its generalization for smart structure modelling. Part I - Solid-shell element formulation. *International Journal for Numerical Methods in Engineering*, 48(4):545–564, 2000.

[20] T. Willmann, S. Bieber, and M. Bischoff. Investigation and elimination of nonlinear poisson stiffening in 3d and solid shell finite elements. *International Journal for Numerical Methods in Engineering*, 124(1):235–263, 2023.

[21] G. Zagari, A. Madeo, R. Casciaro, S. De Miranda, and F. Ubertini. Koiter analysis of folded structures using a corotational approach. *International Journal of Solids and Structures*, 50(5):755–765, 2013.